INSTITUTE OF PHYSICS PUBLISHING JOURNAL OF PHYSICS B: ATOMIC, MOLECULAR AND OPTICAL PHYSICS

J. Phys. B: At. Mol. Opt. Phys. **39** (2006) 1625–1637 doi:10.1088/0953-4075/39/7/006

Applications and implementation of Fourier multiport devices

S Zhang[1], C Lei[1], A Vourdas[1] and J A Dunningham[2]

[1] Department of Computing, University of Bradford, Bradford BD7 1DP, UK
[2] School of Physics and Astronomy, University of Leeds, Leeds LS2 9JT, UK

Received 7 December 2005
Published 13 March 2006
Online at stacks.iop.org/JPhysB/39/1625

Abstract

Fourier multiport devices in which the creation and annihilation operators at the output are related to those at the input through a finite Fourier transform are studied. A general method for the calculation of the output for arbitrary input states is presented. The case of a squeezed state at one of the inputs and vacua at all other inputs is discussed. In the case of thermal states at the input, the device can be used as a thermometer. A factorization technique inspired by the fast Fourier transform leads to a substantial reduction in the number of beam splitters that are required for the experimental implementation of these devices.

(Some figures in this article are in colour only in the electronic version)

1. Introduction

Multiport devices are of great interest from both a theoretical and a practical point of view. Mach–Zehnder interferometers, for example, have been studied extensively [1–3, 5–9, 17] and can be used for precise measurements (e.g., in optical gyroscopes, in gravitational wave detectors, etc). Other multiport devices have also been studied in the literature for both photons and atoms [10–14]. Multiport devices with six or eight ports have been experimentally demonstrated in [15]. These devices perform unitary transformations and could be used as gates in quantum information processing schemes.

In a recent paper [16], the Fourier multiport devices have been studied, where the creation and annihilation operators $\{a_M^\dagger, a_M\}$ at the d inputs are related to the creation and annihilation operators $\{A_M^\dagger, A_M\}$ at the d outputs through a finite Fourier transform. A theoretical formalism for the operation of this device has been developed, with emphasis on novel uncertainty relations which connect the distribution of photons in the various modes at the input, with the correlations between the various modes at the output.

In this paper, we study different aspects of these devices. We first present two different methods for the calculation of the states at the output, for arbitrary states at the input. The first

method is based on a decomposition of the states at the input into eigenstates of the unitary operator U_F that describes the device. For coherent states at the input we show that we also get coherent states at the output, and our second method uses a decomposition of the states at the input into coherent states.

We consider two important examples. In the first one, we have a squeezed state at one of the inputs and vacua at all the other inputs. We show that the output states are entangled.

In the second example, we have thermal states at all inputs. An interesting case is when all these states apart from one have equal temperature which is known. This device can be used as a 'thermometer' to measure the unknown temperature.

The Fourier multiport device can be realized with $\frac{d(d-1)}{2}$ beam splitters in conjunction with appropriate wave plates to adjust phases [10]. Clearly, for large d a large number of optical components are required. Here we propose a scheme for the reduction in the number of optical components at large d. The scheme is based on the 'fast Fourier transform' method which factorizes appropriately large Hilbert spaces as tensor products of smaller ones. The Fourier transform is performed in the smaller spaces and the results are appropriately combined to produce the Fourier transform in the large space. This is extensively used in numerical calculations of Fourier transforms, in order to reduce the computation time. Here we use a similar scheme to reduce the number of beam splitters. There are many fast Fourier transform schemes [18], and we use that by Good which is based on a factorization of d as $d = d_1 \times \cdots \times d_N$, where the factors $d_1, \ldots, d_N$ are coprime with respect to each other.

2. Fourier multiport devices

We consider a $2d$-port device (with d inputs and d outputs). We use the notation

$$a_M = \mathbf{1} \otimes \cdots \otimes a \otimes \cdots \otimes \mathbf{1}, \qquad a_M^\dagger = \mathbf{1} \otimes \cdots \otimes a^\dagger \otimes \cdots \otimes \mathbf{1} \tag{1}$$

for the annihilation and creation operators of photons at the Mth input, where the indices are integers modulo d. They satisfy the commutation relations $\left[a_M, a_K^\dagger\right] = \delta(M, K)$, where $\delta(M, K)$ is Kronecker's delta (it is equal to 1 when $M = K$ (modulo d)).

A Fourier multiport device performs the unitary transform

$$\begin{aligned} U_F &\equiv \exp\left[-\sum_{M,K} a_M^\dagger (\ln F)_{MK} a_K\right], \\ F_{MK} &= d^{-1/2}\omega^{MK}, \qquad \omega = \exp\left(\mathrm{i}\frac{2\pi}{d}\right). \end{aligned} \tag{2}$$

We use the notation A_M and $A_M^\dagger$ for the annihilation and creation operators of photons at the output, and we get

$$A_M = U_F a_M U_F^\dagger = d^{-1/2} \sum_K a_K \omega^{KM}, \tag{3}$$

and similarly for $A_M^\dagger$. We note that

$$\sum_M A_M^\dagger A_M = \sum_M a_M^\dagger a_M, \tag{4}$$

and therefore the average number of photons at the output of this device is equal to the average number of photons at the input. This is of course a general feature of passive linear optical devices.

2.1. Eigenstates of U_F

F is a $d \times d$ unitary matrix which performs a finite Fourier transform in the context of finite quantum systems. We diagonalize the matrix $\mathrm{i} \ln F$ as follows:

$$\mathrm{i} \ln F = W^{\dagger} E W, \qquad E = \mathrm{diag}(\epsilon_0, \ldots, \epsilon_{d-1}). \tag{5}$$

The matrix F has the eigenvalues $1, \mathrm{i}, -1, -\mathrm{i}$, with multiplicities given in [20]. Consequently, the eigenvalues ϵ_M of $\mathrm{i} \ln F$ take the values $\pi/2, 0, (-\pi)/2, -\pi$. As an example, we give in the appendix the matrices W and E, for $d = 5$.

We now introduce the creation and annihilation operators

$$b_M = \sum_K W_{MK} a_K, \qquad b_M^{\dagger} = \sum_K W_{MK}^{*} a_K^{\dagger} \tag{6}$$

and the corresponding number states

$$|N_0, \ldots, N_{d-1}\rangle_b \equiv \frac{\left(b_0^{\dagger}\right)^{N_0}}{N_0^{1/2}} \cdots \frac{\left(b_{d-1}^{\dagger}\right)^{N_{d-1}}}{N_{d-1}^{1/2}} |0, \ldots, 0\rangle. \tag{7}$$

They are eigenstates of the operator U_F:

$$U_F |N_0, \ldots, N_{d-1}\rangle_b \equiv \exp\left(\mathrm{i} \sum_M \epsilon_M N_M\right) |N_0, \ldots, N_{d-1}\rangle_b. \tag{8}$$

Therefore, when these states enter the device, they exit with a trivial phase factor.

2.2. States at the output

Here we assume a general state $|s\rangle$ at the input of the Fourier multiport device and calculate the state at the output. We present two different methods. In the first method, we expand $|s\rangle$ in the basis of equation (7):

$$|s\rangle = \sum s(N_0, \ldots, N_{d-1}) |N_0, \ldots, N_{d-1}\rangle_b. \tag{9}$$

It is easily seen that the state at the output of the device is

$$|S\rangle \equiv U_F |s\rangle = \sum \exp\left(\mathrm{i} \sum_M \epsilon_M N_M\right) s(N_0, \ldots, N_{d-1}) |N_0, \ldots, N_{d-1}\rangle_b. \tag{10}$$

The second method is to expand the state $|s\rangle$ into coherent states. For coherent states at the input, the output states are also coherent states

$$|A_0, \ldots, A_{d-1}\rangle \equiv U_F |\alpha_0, \ldots, \alpha_{d-1}\rangle, \qquad A_M = d^{-1/2} \sum_K \omega^{-MK} \alpha_K. \tag{11}$$

Equation (3) has been used in the proof of this relation. A consequence of this is that for an arbitrary input pure state $|s\rangle$

$$\begin{aligned} |s\rangle &= \left(\frac{1}{\pi}\right)^d \int s(\alpha_0, \ldots, \alpha_{d-1}) |\alpha_0, \ldots, \alpha_{d-1}\rangle \, \mathrm{d}\alpha_0 \cdots \mathrm{d}\alpha_{d-1}, \\ s(\alpha_0, \ldots, \alpha_{d-1}) &= \langle \alpha_0, \ldots, \alpha_{d-1} | s \rangle, \end{aligned} \tag{12}$$

the output is

$$\begin{aligned} |S\rangle = U_F |s\rangle &= \left(\frac{1}{\pi}\right)^d \int S(A_0, \ldots, A_{d-1}) |A_0, \ldots, A_{d-1}\rangle \, \mathrm{d}A_0 \cdots \mathrm{d}A_{d-1}, \\ S(A_0, \ldots, A_{d-1}) &= s(\alpha_0, \ldots, \alpha_{d-1}), \end{aligned} \tag{13}$$

and A_i are related to α_j through the Fourier transform of equation (11).

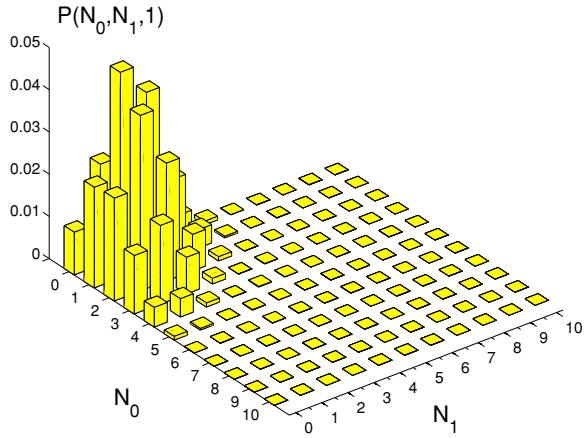

Figure 1. The probabilities $p(N_0, N_1, 1)$ for the state at the output. At the input we have a squeezed state with $\xi = 0.5$ and $\langle N\rangle = 4$ in the $K = 1$ mode and vacua in the other two modes.

3. A squeezed state and vacua at the input

Let

$$D(\alpha) = \exp(\alpha a^\dagger - \alpha^* a), \tag{14}$$

$$S(\xi) = \exp\left[\tfrac{1}{2}(\xi^* a^2 - \xi a^{\dagger 2})\right] \tag{15}$$

be the displacement and squeezing operators, respectively. A single-mode squeezed state is defined as

$$\begin{aligned} &|\alpha, \xi\rangle = D(\alpha)S(\xi)|0\rangle = S(\xi)D(\beta)|0\rangle, \\ &\alpha = \beta\cosh(|\xi|) - \beta^* e^{i\theta}\sinh(|\xi|), \qquad \theta = \arg(\xi). \end{aligned} \tag{16}$$

We assume that the K input mode is in a squeezed state and all other ones are in vacua.

$$|s\rangle = \exp\left(\alpha a_K^\dagger - \alpha^* a_K\right)\exp\left[\tfrac{1}{2}\left(\xi^* a_K^2 - \xi a_K^{\dagger 2}\right)\right]|0, \ldots, 0\rangle. \tag{17}$$

The output state in this case is

$$|S\rangle = \exp\left(\alpha A_K^\dagger - \alpha^* A_K\right)\exp\left[\tfrac{1}{2}\left(\xi^* A_K^2 - \xi A_K^{\dagger 2}\right)\right]|0, \ldots, 0\rangle. \tag{18}$$

As an example, we consider the case $d = 3$ with the squeezed state in the $K = 1$ mode and vacua in the $0, 2$ modes. In all our numerical results, the squeezed states have an average number of four photons, and therefore according to equation (4) the output state also has a total average number of four photons. In the numerical work, we truncated each of the three Hilbert spaces at $N_{\max} = 10$ so that the average number of photons in each mode is much smaller than $N_{\max}$. We consider the case of real ξ, and then the average number of photons in the squeezed state is

$$\langle N\rangle = |\alpha|^2 + \sinh^2(|\xi|). \tag{19}$$

We have calculated the probability distribution

$$p(N_0, N_1, N_2) = |\langle N_0, N_1, N_2|S\rangle|^2. \tag{20}$$

Results for $\xi = 0.5$ are shown in figure 1 for $N_0 = 1$. Since the total average number of photons is 4, it is seen that the probabilities are practically zero when any of the N_0, N_1, N_2

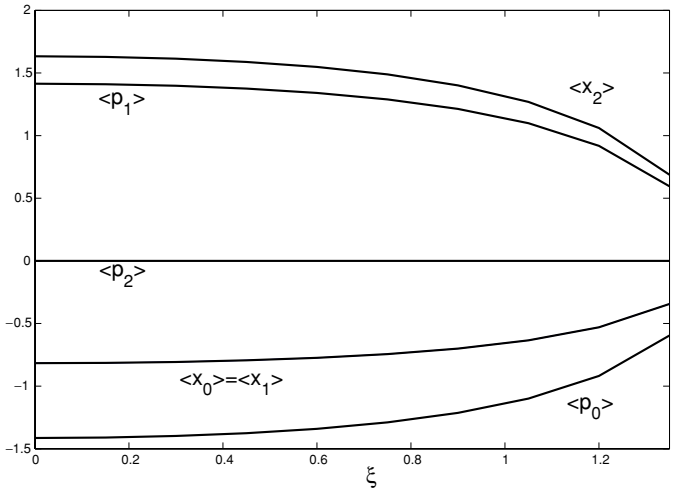

Figure 2. The average positions and momenta as functions of ξ for the states at the output. At the input we have a squeezed state with $\langle N\rangle = 4$ in the $K = 1$ mode and vacua in the other two modes.

gets close to $N_{\max} = 10$. Therefore, the truncation at $N_{\max} = 10$ is sufficient for a good approximation.

We next introduce the conjugate variables

$$x_M = 2^{-1/2}\big[a_M^\dagger + a_M\big], \qquad p_M = 2^{-1/2}\mathrm{i}\big[a_M^\dagger - a_M\big]. \tag{21}$$

In an optical context, they are the magnetic and electric fields, and they are analogous to position and momentum of the harmonic oscillator.

We have also calculated the following average positions and their uncertainties:

$$\langle x_i\rangle = \langle S|x_i|S\rangle, \qquad \big\langle x_i^2\big\rangle = \langle S|x_i^2|S\rangle, \qquad \Delta x_i = \big[\big\langle x_i^2\big\rangle - \langle x_i\rangle^2\big]^{1/2} \tag{22}$$

and also the corresponding average momenta and their uncertainties. Results are given in figures 2 and 3 for various real values of ξ. In figure 2, it is seen that

$$\langle x_0\rangle + \langle x_1\rangle + \langle x_2\rangle = 0, \qquad \langle p_0\rangle + \langle p_1\rangle + \langle p_2\rangle = 0. \tag{23}$$

This is explained if we use equation (3) to show that $x_0 = \sum_M U_F^\dagger x_M U_F$, and similarly for the momentum. The fact that we have a vacuum at the zero input mode leads to the result of equation (23). In figure 3, it is seen that $(\Delta x_2)^2$ takes values less than $1/2$ which indicates squeezing in mode 2. So at the input we have a squeezed state in the mode $K = 1$ and at the output we have a squeezed state in the mode $K = 2$. We note that although the inputs are the same in the 0, 2 modes, their outputs are different. This is because

$$A_0 = 3^{-1/2}[a_0 + a_1 + a_2], \qquad A_2 = 3^{-1/2}[a_0 + a_1\omega^2 + a_2\omega], \qquad \omega = \exp\left(\mathrm{i}\frac{2\pi}{3}\right). \tag{24}$$

From the full density matrix $R = |S\rangle\langle S|$, we calculate the reduced density matrices

$$R_{ij} = \mathrm{Tr}_k R, \qquad R_i = \mathrm{Tr}_{jk} R, \qquad i, j, k = 0, 1, 2, \tag{25}$$

and calculate the entropic quantities $S(R_i)$ and

$$I_{ij} = S(R_i) + S(R_j) - S(R_{ij}), \tag{26}$$

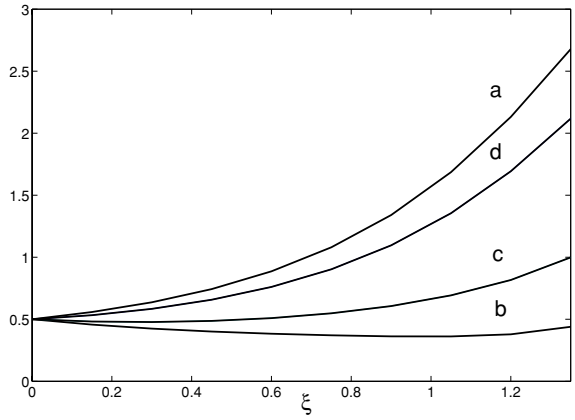

Figure 3. The uncertainties in positions and momenta as functions of ξ for the states at the output. At the input we have a squeezed state with $\langle N\rangle = 4$ in the $K = 1$ mode and vacua in the other two modes. Curve (a) shows $(\Delta p_2)^2$, curve (b) shows $(\Delta x_2)^2$, curve (c) shows $(\Delta p_0)^2 = (\Delta p_1)^2$ and curve (d) shows $(\Delta x_0)^2 = (\Delta x_1)^2$. The output state at the $K = 2$ mode has uncertainty $(\Delta x_2)^2 < 1/2$ (squeezing).

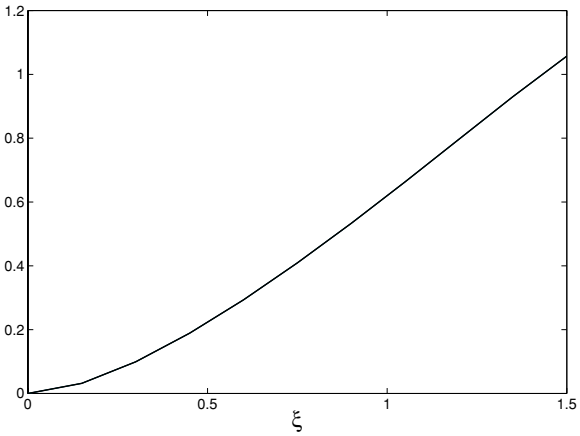

Figure 4. The entropic quantities $S(R_0) = S(R_1) = S(R_2) = I_{01} = I_{02} = I_{12}$ at the output against the squeezing parameter ξ. At the input we have a squeezed state with $\langle N\rangle = 4$ in the $K = 1$ mode and vacua in the other two modes.

where $S(\rho) = -\mathrm{Tr}\,\rho \ln \rho$ is the von Neumann entropy. For the example considered, we found

$$S(R_0) = S(R_1) = S(R_2) = I_{01} = I_{02} = I_{12}. \tag{27}$$

Numerical results for this quantity are shown in figure 4. It is seen that the entropies $S(R_0) = S(R_1) = S(R_2)$ are non-zero, which shows that R_0, R_1, R_2 are mixed states. Since the full state R at the output is a pure state, we conclude that it is an entangled state and the entropies presented can be used as measures of entanglement.

We note that other devices which involve beam splitters and have squeezed states at the input can also produce entangled states at the output [17].

4. Thermal states at the inputs

In this section, we consider thermal states with different temperatures at the various inputs:

$$\rho = \mathcal{N} \exp\left(-\sum_M \beta_M a_M^\dagger a_M\right), \qquad \mathcal{N} = \prod_M (1 - \mathrm{e}^{-\beta_M}), \tag{28}$$

where $\beta_M = (k_B T_M)^{-1}$. In this case, the output is described with the density matrix

$$U_F \rho U_F^\dagger = \mathcal{N} \exp\left[-d^{-1/2} \sum_{K,\Lambda} \tilde{\beta}_{K-\Lambda} a_K^\dagger a_\Lambda\right], \qquad \tilde{\beta}_N = d^{-1/2} \sum_M \beta_M \omega^{-MN}. \tag{29}$$

In the special case that all inverse temperatures are equal to each other

$$\rho_{\mathrm{th}}(\beta) = \mathcal{N}_0 \exp\left(-\beta \sum_M a_M^\dagger a_M\right), \qquad \mathcal{N}_0 = (1 - \mathrm{e}^{-\beta})^d, \tag{30}$$

the output is exactly the same density matrix. In this case, we simply have thermal noise at the input and thermal noise at the output.

We next consider the case when all the inputs are thermal states with the same inverse temperature β, except the K mode where the inverse temperature is $\beta + \lambda$. The density matrix is

$$\rho = \mathcal{N}_1 \mathcal{N}_0 \exp\left[-\lambda a_K^\dagger a_K - \sum_M \beta a_M^\dagger a_M\right], \qquad \mathcal{N}_1 = \frac{1 - \mathrm{e}^{-\beta-\lambda}}{1 - \mathrm{e}^{-\beta}}. \tag{31}$$

Using the general result of equation (29), we find that the density matrix at the output is

$$R \equiv U_F \rho U_F^\dagger = \rho_{\mathrm{th}}(\beta) \mathcal{N}_1 \exp\left[-\frac{\lambda}{d} \sum_{M,N} \omega^{KN} a_M^\dagger a_{M-N}\right]. \tag{32}$$

As an example, we have chosen $d = 3, K = 1, \beta = \ln(1.75)$ and $\lambda = 0.4$ and we have calculated the probability distribution

$$p(N_0, N_1, N_2) = \langle N_0, N_1, N_2 | R | N_0, N_1, N_2 \rangle. \tag{33}$$

Results are shown in figure 5 for $N_2 = 0$. It is seen that the probabilities are practically zero when any of the N_0, N_1, N_2 gets close to $N_{\max} = 10$. Therefore, the truncation at $N_{\max} = 10$ is sufficient for a good approximation.

We have also calculated the entropic quantities of equation (26). We find that $I_{01} = I_{02} = I_{12}$. The numerical values shown in figure 6 indicate that when $\lambda \neq 0$ the outputs are correlated. This is not surprising because although at the various inputs we have thermal noise, there is information in the fact that the temperatures are different and this leads to nontrivial results (correlations between the various outputs).

4.1. Fourier multiport devices as thermometers

This device can be used as a 'thermometer' for thermal states as follows. For small values of λ/d, we can approximate equation (32) with

$$R = U_F \rho U_F^\dagger \approx \rho_{\mathrm{th}}(\beta) \mathcal{N}_1 \left[\mathbf{1} - \frac{\lambda}{d} \sum_{M,N} \omega^{KN} a_M^\dagger a_{M-N}\right]. \tag{34}$$

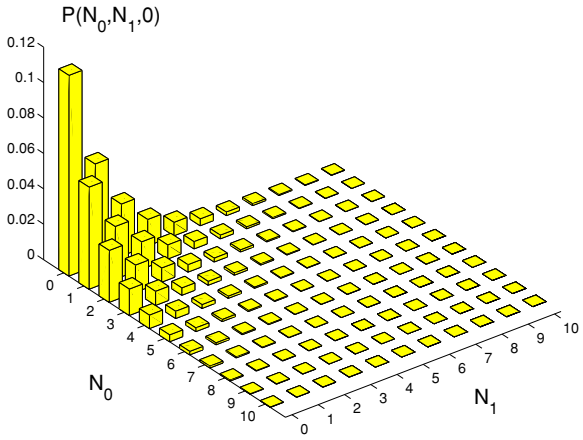

Figure 5. The probabilities $p(N_0, N_1, 0)$ for the state at the output. At the input we have thermal states with inverse temperature $\beta = \ln(1.75)$ in the $K = 0, 2$ modes, and a thermal state with inverse temperature $\beta + \lambda$ (with $\lambda = 0.4$) in the $K = 1$ mode.

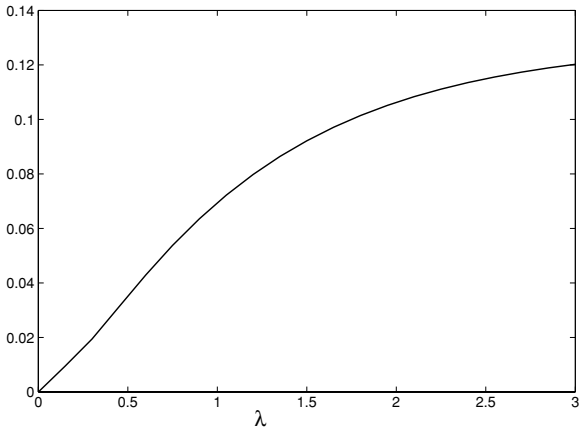

Figure 6. The entropic quantities $I_{01} = I_{02} = I_{12}$ as functions of λ at the output. The input is the same as in figure 5.

Using this we have calculated the reduced density matrix at the zero mode at the output

$$R_0 = \mathrm{Tr}_{1\ldots(d-1)} R = \mathcal{N}_1 \rho_{\mathrm{th}}^{(0)}(\beta) \left[1 - \frac{\lambda}{d} a_0^\dagger a_0 - (d-1)(\mathrm{e}^\beta - 1)^{-1} \right], \qquad \rho_{\mathrm{th}}^{(0)}(\beta) = (1 - \mathrm{e}^{-\beta}) \exp\left(-\beta a_0^\dagger a_0\right) \tag{35}$$

and the corresponding second-order correlation

$$g_0^{(2)} = \frac{\mathrm{Tr}\left[R_0 \left(a_0^\dagger\right)^2 a_0^2\right]}{\left[\mathrm{Tr}\, R_0 a_0^\dagger a_0\right]^2}. \tag{36}$$

Results are shown in figure 7. In order to use this device as a thermometer of thermal states, we input the thermal state whose temperature we want to measure at the zero mode, and we input thermal states of equal known inverse temperature β at the modes $1, \ldots, d-1$. We then measure $g^{(2)} - 2$ at the output of the zero mode. Non-zero value of this indicates deviation

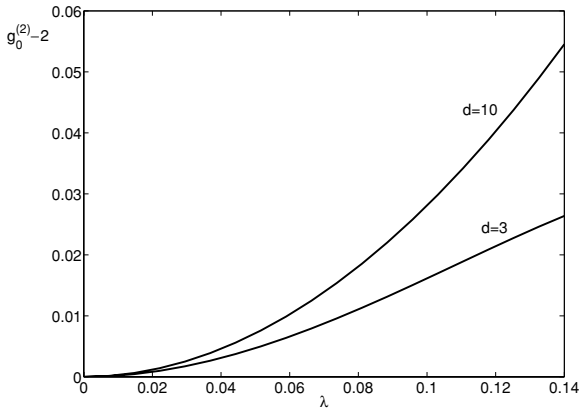

Figure 7. The second-order correlation $g_0^{(2)} - 2$ as a function of λ at the output of the $K = 0$ mode. At the input we have thermal states with inverse temperature $\beta = \ln 2$ in the $K = 1, \ldots, d-1$ modes, and a thermal state with inverse temperature $\beta + \lambda$ in the $K = 0$ mode. The curves shown are for $d = 3$ and $d = 10$. The curves can be used to determine the temperature of the input thermal state at the $K = 0$ mode. The accuracy of the device increases with d.

from the thermal state. Figure 7 can be used to find the unknown temperature. The slope of the curves in figure 7 increases as a function of d, and therefore the accuracy of the thermometer increases with d. This can be understood from equation (35) which shows that for a given λ, the probabilities $\langle N|R_0|N\rangle$ with large N are increasing functions of d. Therefore, as d increases, the distribution becomes wider and $g^{(2)} - 2$ increases.

5. Fourier multiport devices with a small number of beam splitters

Fourier multiport devices can be implemented with $d(d-1)/2$ beam splitters [10]. For large d, this requires a very large number of beam splitters. In this section, we propose a scheme for the reduction in the number of beam splitters. Our scheme is inspired by the 'fast Fourier transform' philosophy where a large Fourier transform is decomposed into many smaller ones, and this substantially reduces the computation time. In our context, this decomposition will enable us to greatly reduce the number of beam splitters required in implementing large Fourier devices, and therefore make them much more realistic prospects in the laboratory. There are many fast Fourier transform methods [18]. Here we use the method introduced by Good which is based on the Chinese remainder theorem. This scheme has been used in the context of finite quantum systems in [19].

We first factorize d as $d = d_1 \times \cdots \times d_N$, where the factors $d_1, \ldots, d_N$ are coprime with respect to each other. Following Good, we introduce two one-to-one mappings between $\mathbb{Z}(d)$ and $\mathbb{Z}(d_1) \times \cdots \times \mathbb{Z}(d_N)$. We first introduce the integers r_i and t_i:

$$r_i = \frac{d}{d_i}, \qquad t_i r_i = 1 (\mathrm{mod}\, d_i). \tag{37}$$

Here, t_i is the 'inverse' of r_i within $\mathbb{Z}(d_i)$. Its existence is guaranteed by the fact that r_i and d_i are coprime. We also introduce $s_i = t_i r_i$ in $\mathbb{Z}(d)$.

The first one-to-one mapping between $\mathbb{Z}(d)$ and $\mathbb{Z}(d_1) \times \cdots \times \mathbb{Z}(d_N)$ is

$$K \leftrightarrow (K_1, \ldots, K_N), \qquad K_i = K (\mathrm{mod}\, d_i), \qquad K = \sum_i K_i s_i. \tag{38}$$

The second one-to-one mapping between $\mathbb{Z}(d)$ and $\mathbb{Z}(d_1) \times \cdots \times \mathbb{Z}(d_N)$ is

$$M \leftrightarrow (\bar{M}_1, \ldots, \bar{M}_N), \qquad \bar{M}_i = M t_i (\mathrm{mod}\, d_i), \qquad M = \sum_i \bar{M}_i r_i (\mathrm{mod}\, d_i). \tag{39}$$

The proof that these maps are indeed one-to-one is based on the Chinese remainder theorem.

Two useful formulae are

$$\omega^{r_i s_i} = \omega_i \equiv \exp\left(\mathrm{i}\frac{2\pi}{d_i}\right) \tag{40}$$

and also

$$i \neq j \rightarrow \omega^{r_i s_j} = 1. \tag{41}$$

They can be used to show that

$$\omega^{KM} = \prod_{i=1}^{N} \omega_i^{K_i \bar{M}_i}. \tag{42}$$

Using the mappings (38) and (39), we relabel F_{KM} of equation (2) as

$$F(K_1, \ldots, K_N; \bar{M}_1, \ldots, \bar{M}_N) = F_1(K_1, \bar{M}_1) \times \cdots \times F_N(K_N, \bar{M}_N), \tag{43}$$

where F_i is the $d_i \times d_i$ Fourier matrix with elements

$$F_i(K_i, \bar{M}_i) = d_i^{-1/2} \omega_i^{K_i \bar{M}_i}. \tag{44}$$

It is very important that when K is relabelled according to the map of equation (38) M should be relabelled according to the 'dual map' of equation (39).

In equation (43), we have the tensor product $F_1 \otimes \cdots \otimes F_N$ which can also be written as

$$F_1 \otimes \cdots \otimes F_N = (F_1 \otimes \mathbf{1}_2 \otimes \cdots \otimes \mathbf{1}_N) \times \cdots \times (\mathbf{1}_1 \otimes \cdots \otimes \mathbf{1}_{N-1} \otimes F_N). \tag{45}$$

The matrices on the right-hand side commute with each other and by taking the logarithm we find that

$$\begin{aligned} \ln[F_1 \otimes \cdots \otimes F_N] &= \ln(F_1 \otimes \mathbf{1}_2 \cdots \otimes \mathbf{1}_N) + \cdots + \ln(\mathbf{1}_1 \otimes \cdots \otimes \mathbf{1}_{N-1} \otimes F_N) \\ &= [(\ln F_1) \otimes \mathbf{1}_2 \cdots \otimes \mathbf{1}_N] + \cdots + [\mathbf{1}_1 \otimes \cdots \otimes \mathbf{1}_{N-1} \otimes (\ln F_N)]. \end{aligned} \tag{46}$$

We multiply this equation on the left by $a_M^\dagger \equiv a^\dagger_{(M_1,\ldots,M_N)}$ and on the right by $a_K \equiv a_{(K_1,\ldots,K_N)}$ and we prove that

$$U_F = \prod_{j=1}^{N} U_j, \qquad [U_i, U_j] = 0, \tag{47}$$

where U_j is

$$U_j = \exp\left[-\sum_{M,K} a_M^\dagger (\mathbf{1}_1 \otimes \cdots \otimes (\mathrm{i} \ln F_j) \otimes \cdots \mathbf{1}_N)_{MK} a_K\right]. \tag{48}$$

This contains a d_j-dimensional Fourier transform F_j in tensor product with a d/d_j-dimensional unit matrix. Therefore, practical implementation of this transform will require d/d_j Fourier multiport devices, each of which implements the F_j Fourier transform. The total number of beams splitters in this device is

$$\sum_j \frac{d}{d_j} \frac{(d_j - 1)d_j}{2} = \frac{d}{2} \sum_j (d_j - 1). \tag{49}$$

As an example, we consider the case where $d = 15$, $d_1 = 5$ and $d_2 = 3$. In this case, we find that $r_1 = 3, t_1 = 2, s_1 = 6$ and $r_2 = 5, t_2 = 2, s_2 = 10$. Therefore, $M = 6M_1 + 10M_2$

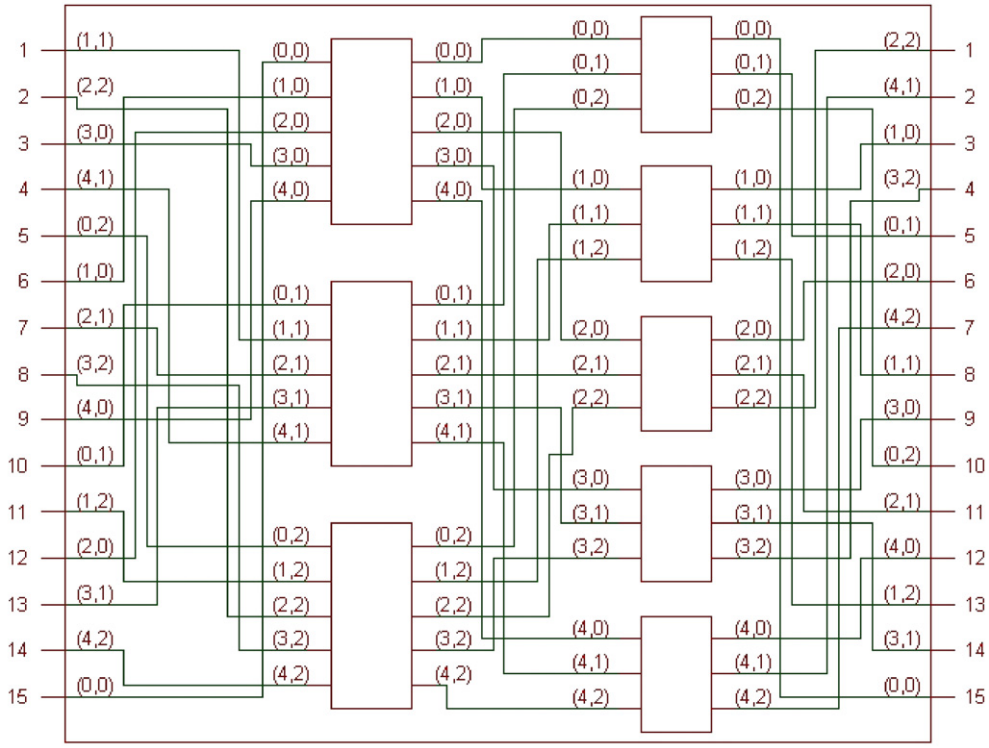

Figure 8. A multiport device with 15 inputs and 15 outputs. According to the fast Fourier transform philosophy, the device is composed of smaller multiport devices. The double labelling of each input as M or equivalently as (M_1, M_2) according to the map $M = 6M_1 + 10M_2$ (equation (38)) is shown in detail. The double labelling of each output as M or equivalently as $(\bar{M}_1, \bar{M}_2)$ according to the dual map of $M = 3\bar{M}_1 + 5\bar{M}_2$ (equation (39)) is also shown in detail.

according to the map of equation (38), and $M = 3\bar{M}_1 + 5\bar{M}_2$ according to the map of equation (39). In figure 8, we draw in detail this device. The double labelling of each input as M or equivalently as (M_1, M_2) according to the map of equation (38) is shown in detail. The double labelling of each output as M or equivalently as $(\bar{M}_1, \bar{M}_2)$ according to the dual map of equation (39) is also shown in detail. We note that in this case the factorization reduces the number of beam splitters from 105 to 45.

6. Discussion

We have considered Fourier multiport devices in which the creation and annihilation operators at the output are related to those at the input, through the finite Fourier transform of equation (3). This device performs the unitary transformation U_F of equation (2). The eigenstates of U_F have been given in equations (6) and (7). They can be used to calculate the states at the output as described in equation (10). An alternative method for the calculation of the states at the output is based on an expansion in terms of coherent states as described in equation (13).

We have studied in detail the case of a squeezed state at one of the inputs and vacua at all the other inputs. The output is an entangled state. Various quantities that characterize the output states have been presented in figures 1–4.

We have also studied the case of thermal states at all inputs. When the temperatures are different, we get correlated states at the various outputs. We have explained how in this case the device can be used as a thermometer. We put the thermal state with the unknown temperature at the zero mode and thermal states of equal temperature at all other modes. Measurement of the second-order correlation $g^{(2)}$ at the zero output gives the unknown temperature as shown in figure 7.

Experimentally, the Fourier multiport device can be realized with $\frac{d(d-1)}{2}$ beam splitters. For large d, it is highly desirable to have a technique which reduces the number of the beam splitters. Inspired by the fast Fourier transform, we have proposed the factorization of equations (47) and (48). Using this factorization, we have designed a Fourier multiport device with 15 inputs and 15 outputs in figure 8.

This work indicates the importance of Fourier multiport devices in modern optical technologies.

Appendix

Using a computer library (e.g., MATLAB), we calculate the unitary matrix W and the diagonal matrix E in equation (5) for $d = 5$:

$$W = \begin{pmatrix} 0.8507 & 0.5257 & 0 & 0.0689 + 0.3075\mathrm{i} & 0 \\ 0.2629 & -0.4253 & 0.6802 & -0.4333 + 0.1900\mathrm{i} & -0.1932 \\ 0.2629 & -0.4253 & -0.1932 & 0.4759 & 0.6802 \\ 0.2629 & -0.4253 & -0.1932 & 0.4759 & -0.6802 \\ 0.2629 & -0.4253 & 0.6802 & -0.4333 + 0.1900\mathrm{i} & 0.1932 \end{pmatrix}, \tag{A.1}$$

$$E = \begin{pmatrix} 0 & 0 & 0 & 0 & 0 \\ 0 & -\pi & 0 & 0 & 0 \\ 0 & 0 & -\frac{\pi}{2} & 0 & 0 \\ 0 & 0 & 0 & 0 & 0 \\ 0 & 0 & 0 & 0 & \frac{\pi}{2} \end{pmatrix}. \tag{A.2}$$

References

[1] Campos R A, Saleh B E A and Teich M C 1989 *Phys. Rev.* A **40** 1371
[2] Holland M J and Burnett K 1993 *Phys. Rev. Lett.* **71** 1355
[3] Hillery M, Zou M and Buzek V 1996 *Quantum Semiclass. Opt.* **8** 1041
[4] Kim T, Pfister O, Holland M J, Noh J and Hall J L 1998 *Phys. Rev.* A **57** 4004
Kim T *et al* 1999 *Phys. Rev.* A **60** 708
[5] Dowling J P 1998 *Phys. Rev.* A **57** 4736
[6] Dunningham J A, Burnett K and Barnett S M 2002 *Phys. Rev. Lett.* **89** 150401
[7] Roberts D C and Burnett K 2003 *Phys. Rev. Lett.* **90** 150401
[8] Shapiro J H, Shepard S R and Wong N C 1989 *Phys. Rev. Lett.* **62** 2377
Schleich W P, Dowling J P and Horowicz R J 1991 *Phys. Rev.* A **44** 3365
Lane A S, Braunstein S L and Caves C M 1993 *Phys. Rev.* A **47** 1667
Campos R A, Gerry C C and Benmoussa A 2003 *Phys. Rev.* A **68** 023810
[9] Lim Y L and Biege A 2005 *Phys. Rev.* A **71** 062311
Lim Y L and Biege A 2005 *New J. Phys.* **7** 155
[10] Reck M, Zeilinger A, Bernstein H J and Bertani P 1994 *Phys. Rev. Lett.* **73** 58
[11] Torma P, Stenholm S and Jex I 1995 *Phys. Rev.* A **52** 4853
Jex I, Stenholm S and Zeilinger A 1995 *Opt. Commun.* **117** 95
Zukowski M, Zeilinger A and Horne M A 1997 *Phys. Rev.* A **55** 2564

[12] Dunningham J A, Burnett K and Phillips W D 2005 *Phil. Trans. R. Soc.* A **363** 2165
[13] Greiner M, Mandel O, Esslinger T, Hansch T W and Bloch I 2002 *Nature* **415** 39
[14] Orzel C, Tuchman A K, Fenselau M L, Yasuda M and Kasevich M A 2001 *Science* **291** 2386
[15] Mattle K, Michler M, Weinfurter H, Zeilinger A and Zukowski M 1995 *Appl. Phys.* B **60** S111
[16] Vourdas A and Dunningham J A 2005 *Phys. Rev.* A **71** 013809
[17] Paris M G A 1999 *Phys. Rev.* A **59** 1615
Kim M S, Son W, Buzek V and Knight P L 2002 *Phys. Rev.* A **65** 032323
[18] McClellan J H and Rader C M 1979 *Number Theory in Digital Signal Processing* (London: Prentice-Hall)
Blahut R E 1985 *Fast Algorithms for Digital Signal Processing* (Reading, MA: Addison-Wesley)
Elliott D F and Rao K R 1982 *Fast Transforms* (London: Academic)
[19] Vourdas A and Bendjaballah C 1993 *Phys. Rev.* A **47** 3523
Vourdas A 2003 *J. Phys. A: Math. Gen.* **36** 5645
[20] Vourdas A 2004 *Rep. Prog. Phys.* **67** 267